BATTERIES

Capacity recovery by transient voltage pulse in silicon-anode batteries

Yufei Yang[1]†, Srija Biswas[1]†, Rong Xu[1], Xin Xiao[1], Xin Xu[1,2], Pu Zhang[1], Huaxin Gong[3], Xueli Zheng[1,4], Yucan Peng[1], Junyan Li[1], Huayue Ai[5], Yecun Wu[1], Yusheng Ye[1], Xin Gao[1], Chad Serrao[1], Wenbo Zhang[1], Philaphon Sayavong[5], Zhuojun Huang[1], Zhouyi Chen[1], Yi Cui[1], Rafael A. Vilá[1], David T. Boyle[5], Yi Cui[1,4,6]*

In the quest for high-capacity battery electrodes, addressing capacity loss attributed to isolated active materials remains a challenge. We developed an approach to substantially recover the isolated active materials in silicon electrodes and used a voltage pulse to reconnect the isolated lithium-silicon (Li_xSi) particles back to the conductive network. Using a 5-second pulse, we achieved >30% of capacity recovery in both Li-Si and Si–lithium iron phosphate (Si-LFP) batteries. The recovered capacity sustains and replicates through multiple pulses, providing a constant capacity advantage. We validated the recovery mechanism as the movement of the neutral isolated Li_xSi particles under a localized nonuniform electric field, a phenomenon known as dielectrophoresis.

The rapid growth of lithium-ion batteries drives the continuous demand for high-capacity electrode materials (*1*–*3*). However, emerging high-capacity materials such as silicon and lithium metal encounter considerable volumetric and structural changes, resulting in the mechanical detachment of active materials (*4*–*6*). The electrochemical isolation of active materials from the bulk electrode or current collector causes substantial capacity decay, hindering the widespread adoption of high-capacity electrodes (*7*–*10*). Li metal anodes often develop dendritic structures (*11*, *12*). When discharging, incomplete stripping results in isolation of the metallic Li from the bulk Li metal electrode or current collectors (*13*–*15*). Similarly, silicon anodes, subjected to 300% volume expansion, experience severe cracking in both particles and electrodes, leading to large quantities of isolated silicon (*16*, *17*). The formation and accumulation of isolated active materials remain primary causes of capacity loss.

Research has examined ways to refine material and electrolyte designs for mitigating capacity fade (*18*–*20*). Strategies such as electrode architecture (*21*–*23*), interfacial modification (*24*–*26*), and electrolyte optimization (*27*–*30*) have yielded substantial progress, particularly in improving interfacial stability. However, the recovery of inactive materials is rarely explored. A series of iodine redox reactions have been designed to chemically rejuvenate dead lithium (*31*). Additionally, a fast-discharging protocol has been introduced to reconnect isolated lithium (*32*). A high current is applied for 1 to 2 min, which induces a dynamic progression during which Li dissolves at one end of the isolated lithium and deposits at the opposite end. The recovery of isolated lithium through resting at a discharged state has been reported, owing to the dissolution of the residual solid electrolyte interphase (SEI), which facilitates the reconnection of isolated lithium (*33*). However, in silicon electrodes, the recovery of lost active materials remains an important yet unexplored topic.

In this work, we developed a process to recover the isolated active materials in silicon electrodes through a short (few seconds) voltage pulse (Fig. 1A). The underlying recovery mechanism is dictated by dielectrophoresis (DEP), which refers to the motion of a neutral particle in a nonuniform electric field. The DEP mechanism was initially applied to biological cells (*34*–*36*) and was subsequently extended to a broader range of materials (*37*–*39*). The DEP force on a particle can be expressed as

$$F_{\mathrm{DEP}} = 2\pi r^3 \varepsilon_{\mathrm{m}} \,\mathrm{Re}[K(\omega)]\nabla E^2$$

where r is the radius of a particle, $K(\omega) = \left(\varepsilon_{\mathrm{p}}^* - \varepsilon_{\mathrm{m}}^*\right)/\left(\varepsilon_{\mathrm{p}}^* + 2\varepsilon_{\mathrm{m}}^*\right)$ is the Clausius-Mossotti factor, and $\varepsilon_{\mathrm{p}}^*$ and $\varepsilon_{\mathrm{m}}^*$ are the complex permittivities of the suspended particle and medium, respectively. The direction of the force is determined by the sign of $\varepsilon_{\mathrm{p}}^* - \varepsilon_{\mathrm{m}}^*$. The force scales with the gradient (∇) of the square of the electric field vector E. DEP theory indicates that neutral particles can move under the electric field when there are (i) polarizability differences between the particle and media and (ii) an electric field gradient.

In our study, isolated Li_xSi (i-Li_xSi) are considered as suspended particles in the electrolyte (el). A direct current pulse is used for which only the real parts of the $\varepsilon_{\mathrm{p}}^*$ and $\varepsilon_{\mathrm{m}}^*$ are considered. In cycled batteries, isolated Li_xSi exhibits different degrees of lithiation, varying from semiconductive Si to metal-like $Li_{15}Si_4$. The range of permittivity allows two conditions of DEP: (i) positive DEP, where ε(i-Li_xSi) > ε(el) i-Li_xSi is highly lithiated and moves toward a higher field density; and (ii) negative DEP, where ε(i-Li_xSi) < ε(el), when i-Li_xSi is barely lithiated and moves toward a lower field density (Fig. 1B). In addition, a voltage pulse applied onto a rugged electrode generates an uneven electric field within the electrode (Fig. 1C and fig. S1). The electric field gradient facilitates the i-Li_xSi movement under the influence of the DEP force, which is either positive or negative based on the lithiation degree of i-Li_xSi, resulting in potential reconnection to other active particles in the electrode.

Pulse protocol and capacity recovery

We investigated the effect of pulse application on cell performance by first using Li metal as the counter electrode. A 4-V constant-voltage pulse was applied to the Si side for 5 s at the end of the delithiation after several cycles (Fig. 2A). We chose 4 V as the maximum integral value within the electrolyte stability range and 5 s to keep the pulse short but sufficient for recovery. At the end of the delithiation, the positive voltage on the Si side drove lithium ion migration away from Si, preventing cell shorting and Li metal plating. We first applied a pulse of 4 V for 5 s at the 20th cycle (Fig. 2B). The cell underwent considerable capacity decay through the initial 20 cycles, and large quantities of isolated Li_xSi were expected. After the pulse application, a 31.0% increase of delithiation capacity, from 1.1004 to 1.4413 mA·hour cm^{-2}, was observed in the subsequent cycle compared with the previous cycle. Furthermore, this increased capacity could be retained through later cycles. Figure 2C outlines the voltage-capacity profile before and after the pulse, where the step order is indicated by numbers. The pulse was applied at the end of delithiation (step 2). In the following lithiation (step 3) and delithiation (step 4), capacity recovery was observed in both steps. The increased lithiation capacity corresponds to the reactivated Si sites in isolated Li_xSi, which can uptake more lithium during lithiation, whereas the increased delithiation capacity corresponds to the reactivated Li in isolated Li_xSi. The statistical analysis highlights the repeatability of the process (Fig. 2D). An average recovered capacity of 0.367 ± 0.046 mA·hour cm^{-2} and recovery rate of 35.6 ± 5.32%, which compares the delithiation capacity in the postpulse cycle to the prepulse cycle, are reported across five parallel cells.

More investigations were conducted to understand the pulse process. The Li stripping capacity during the 5-s pulse was calculated to be only ~0.06 mA·hour cm^{-2} from the current-time

[1]Department of Materials Science and Engineering, Stanford University, Stanford, CA 94305, USA. [2]The Polytechnic School, Ira A. Fulton Schools of Engineering, Arizona State University, Mesa, AZ 85212, USA. [3]Department of Chemical Engineering, Stanford University, Stanford, CA 94305, USA. [4]Stanford Institute for Materials and Energy Sciences, SLAC National Accelerator Laboratory, Menlo Park, CA 94025, USA. [5]Department of Chemistry, Stanford University, Stanford, CA 94305, USA. [6]Department of Energy Science and Engineering, Stanford University, Stanford, CA 94305, USA.
*Corresponding author. Email: yicui@stanford.edu
†These authors contributed equally to this work.

profile, indicating that the pulse itself contributes minor capacity (fig. S2A). Scanning electron microscopy (SEM) studies showed no observable additional Li chunks on either the Si surface or Li metal surface (fig. S3). The interfacial properties were carefully characterized. The impedance measurements revealed similar ohmic resistance (R_{ohm}) and SEI resistance (R_{SEI}) before and after the pulse (fig. S2, B and C). X-ray photoelectron spectroscopy (XPS) results for both Si (fig. S4) and Li (fig. S5) showed minor differences of the SEI components before and after the pulse. Cryo–transmission electron microscopy (cryo-TEM) studies measured a similar SEI thickness of ~50 nm in the pre- and postpulse samples and revealed no visible morphological differences in the SEI (fig. S6). We also applied different voltages and pulse durations at the 20th cycle for recovery (fig. S7). When we varied the voltage from 2 to 6 V, we observed more recovery at higher voltage. When we extended the pulse duration from 1 to 5 s, we observed more recovery. After 5 s, a saturation effect was observed such that 10- and 5-s pulses gave equal recovery. This saturation is possibly because 5 s of movement is sufficient for particle reconnection within densely packed electrodes. To provide a more comprehensive understanding, we investigated the effects of pulse application on isolated lithium (fig. S8). Our findings indicate that pulse application can facilitate the reconnection of isolated Li but the efficacy of this process is constrained by the inherent properties of Li metal electrodes.

With increased cycles, electrode deteriorative fracturing and accumulation of SEI aggravate active Si loss, leading to the final rapid capacity decay. In the end-of-life state, we applied the same 4-V, 5-s pulse at the 200th cycle to recover the capacity loss from the isolated Li_xSi (Fig. 2E and fig. S9A). A high recovery rate of 138.8%, from 0.2799 to 0.6683 mA·hour cm^{-2}, was obtained because huge amounts of isolated Li_xSi had accumulated after 200 cycles. The recovered capacity was retained in the following cycles, though it experienced decay, possibly owing to severe mechanical instability in the end-of-life state. The pulse was also applied to the intermediate cycling state, where the silicon electrode had undergone numerous cycles but had not yet reached its end-of-life state. The 4-V, 5-s pulse at the 80th cycle achieved capacity recovery of 32.1%, from 0.9397 to 1.2416 mA·hour cm^{-2} (fig. S9, B and C). Additionally, we studied the effect of multiple pulses during the initial cycles by applying pulses at the 5th, 10th, 15th, 20th, and 25th cycles (Fig. 2F). The pulses at the 5th and 10th cycles showed bare recovery when the capacity substantially dropped. This phenomenon is likely attributable to the substantial volume fluctuations during the initial cycles, which renders the unstable reconnection of isolated Li_xSi particles. However, the pulses at the 5th and 10th cycles mitigated the rate of capacity degradation (fig. S10). As the capacity degradation began to stabilize, the capacity recovery by the pulse became evident. The pulse at the 15th, 20th, and 25th cycles achieved capacity recoveries of 5.0, 7.5, and 7.1%, respectively. At the 25th cycle, the cell to which multiple pulses were applied demonstrated a more than 30% capacity improvement compared with a control cell that did not receive pulse application. This capacity improvement persisted for more than 100 cycles, establishing the practical aspect of the voltage pulse application.

Mechanism verification

To confirm the contribution of isolated Li_xSi in the capacity recovery, we designed a constant current–constant voltage (CCCV) testing protocol combined with titration-gas chromatography (TGC). In the CCCV testing protocol, a CV delithiation step was added after each regular CC delithiation. The goal of this CV step was to maximize removal of the trapped Li capacity in the active Si. At the end of the CV delithiation, a 4-V, 5-s pulse was applied and resulted in a 102.6% recovery in delithiation capacity, from 0.5903 to 1.1961 mA·hour cm^{-2}. This substantial recovery after maximum delithiation of the trapped Li indicates that the trapped Li in the active Si barely contributes to the capacity recovery (Fig. 3A). In the cycle after the pulse, the lithiation and delithiation capacity increased by 0.372 and 0.233 mA·hour cm^{-2}, corresponding to the quantity of Si capacity and the quantity of Li capacity in the recovered isolated Li_xSi, respectively. For further verification, TGC was conducted to assess the quantity of isolated Li_xSi. Here, we chose a mild protic solvent, ethanol, to react with Li_xSi, but not SEI, and generate H_2 for Li quantification

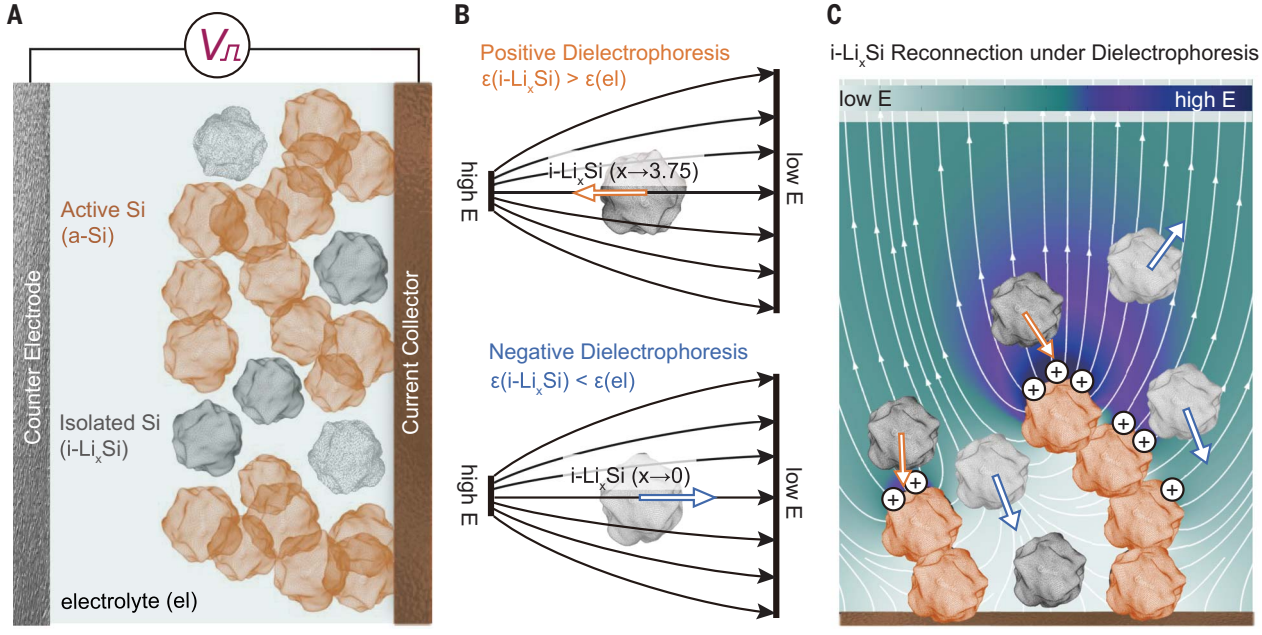

Fig. 1. Reconnection of isolated Si under dielectrophoretic force. (**A**) Voltage-pulse application onto a cycled Si electrode. The electrode accumulates isolated Si (i-Li_xSi) with different degrees of lithiation. (**B**) Schematic illustration of positive DEP and negative DEP. (**C**) The simulated electric field distribution within Si electrodes after pulse application and the resultant movement of isolated Si under DEP. The color contour illustrates the electric field density, and white lines with arrows show the electric field lines.

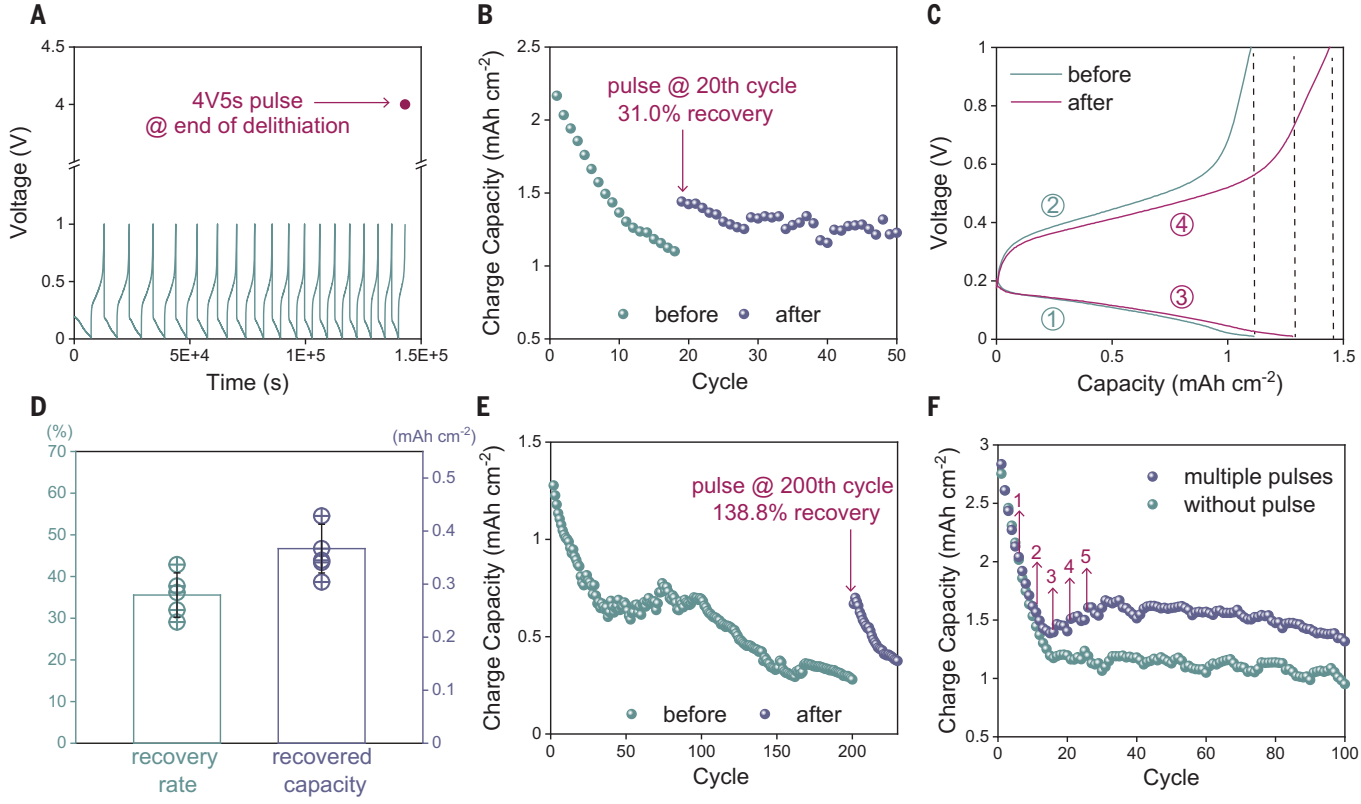

Fig. 2. Capacity recovery through the voltage pulse. (**A**) Voltage-time profiles of Li-Si cells, illustrating the pulse-application profile. (**B**) Capacity recovery of Li-Si half cells with one 4-V, 5-s pulse at the 20th cycle (two preactivation cycles are not included in the graph). (**C**) Voltage-capacity profiles of Li-Si cells before and after the 4-V, 5-s pulse at the 20th cycle. The order is indicated by numbers. The vertical dashed lines are drawn to guide the eye. (**D**) Recovery rate and recovered capacity (defined by comparing the delithiation capacity in the postpulse cycle to the prepulse cycle) by the 4-V, 5-s voltage pulse. Each colored circle represents one cell, the box shows the average value, and the error bars indicate the standard deviation. (**E**) Capacity recovery of Li-Si half cells with one 4-V, 5-s pulse at the 200th cycle (two preactivation cycles are not included in the graph). (**F**) Capacity of Li-Si half cells without a pulse and with five 4-V, 5-s pulses at the 5th, 10th, 15th, 20th, and 25th cycles, respectively (two preactivation cycles are not included in the graph). The numbers indicate the sequence of the pulses.

(*40*, *41*) (Fig. 3B). We performed TGC after the CV steps in the cycle before the pulse (state A) and after the pulse (state B). Because the CV steps had maximumly delithiated the trapped Li in the active Si, the remaining Li capacity predominately resided within the isolated Li_xSi. The TGC result at state A thus represents the Li quantity in the accumulated i-Li_xSi, whereas the TGC result at state B represents the Li capacity in the remaining i-Li_xSi after the pulse. Figure 3C demonstrates an average reduction of 0.268 mA·hour cm^{-2} in Li capacity after the pulse. This value measured by TGC corresponds to the Li capacity in the recovered isolated Li_xSi via the pulse, which is consistent with the value (0.233 mA·hour cm^{-2}) measured from the voltage curve. The cross-validation further confirms that isolated Li_xSi primarily contributes to the pulse-induced capacity recovery.

We further verified the reconnection mechanism of DEP. The DEP mechanism is characterized by its interaction with neutral particles, and its force direction is independent of the polarity of the electric field. We first measured the zeta potential of Li_xSi particles dispersed in the electrolyte by phase analysis light scattering (PALS). The Li_xSi particle was scratched off from the cycled Si anode, effectively imitating the isolated Li_xSi in the electrodes. We conducted additional measurements on Si nanoparticles in toluene, which represent particles with bare surface charges, as well as Si nanoparticles in water, which represent charged particles. Figure 3D illustrates that the measured zeta potentials of both i-Li_xSi in the electrolyte and Si nanoparticles in toluene exhibit a substantial variation from positive to negative. This pattern reflects the characteristics of the neutral particles. By contrast, the zeta potential measurement of Si nanoparticles in water (pH = 7) yielded consistent results, averaging at −82.88 mV, which shows that the characteristics of the charged particles are consistent with the literature (*42*). These results support that i-Li_xSi particles barely possess surface charges in the electrolyte. To further validate that the recovery is independent of the polarity of the electric field, we designed a negative-pulse protocol. The negative pulse was conducted at the end of the lithiation to prevent cell shorting (Fig. 3E). A 5-s pulse of negative 4 V at the 20th cycle achieved 36.6% capacity recovery, from 1.3224 to 1.8071 mA·hour cm^{-2}, showing a similar recovery phenomena to that of the positive pulse (Fig. 3F). The Li capacity within the recovered isolated Li_xSi was lower than that obtained with the positive pulse, potentially owing to the domination of barely lithiated i-Li_xSi ($x \rightarrow 0$) in the fully lithiated state (fig. S11). This result demonstrates that the pulse-induced recovery is unaffected by the polarity of the electric field.

To visualize the migration of isolated Li_xSi under the voltage pulse, we first performed in situ SEM to visualize the movement of a single isolated Li_xSi particle under the nonuniform electric field (Fig. 4A and fig. S12). A tungsten (W) tip and a Cu film were used as working and counter electrodes. A Ta-doped $Li_7La_3Zr_2O_{12}$ pellet was chosen as the substrate because it has an electronically insulating nature but barely has a charging effect under the electron beam (*43*). The isolated Li_xSi particle was scratched off from the cycled Si anode. A 10-V constant voltage was applied to the tungsten tip, creating an inhomogeneous electric field between two electrodes, which is the prerequisite for DEP. Under this vacuum condition where ε(i-Li_xSi) > ε(vacuum), a positive

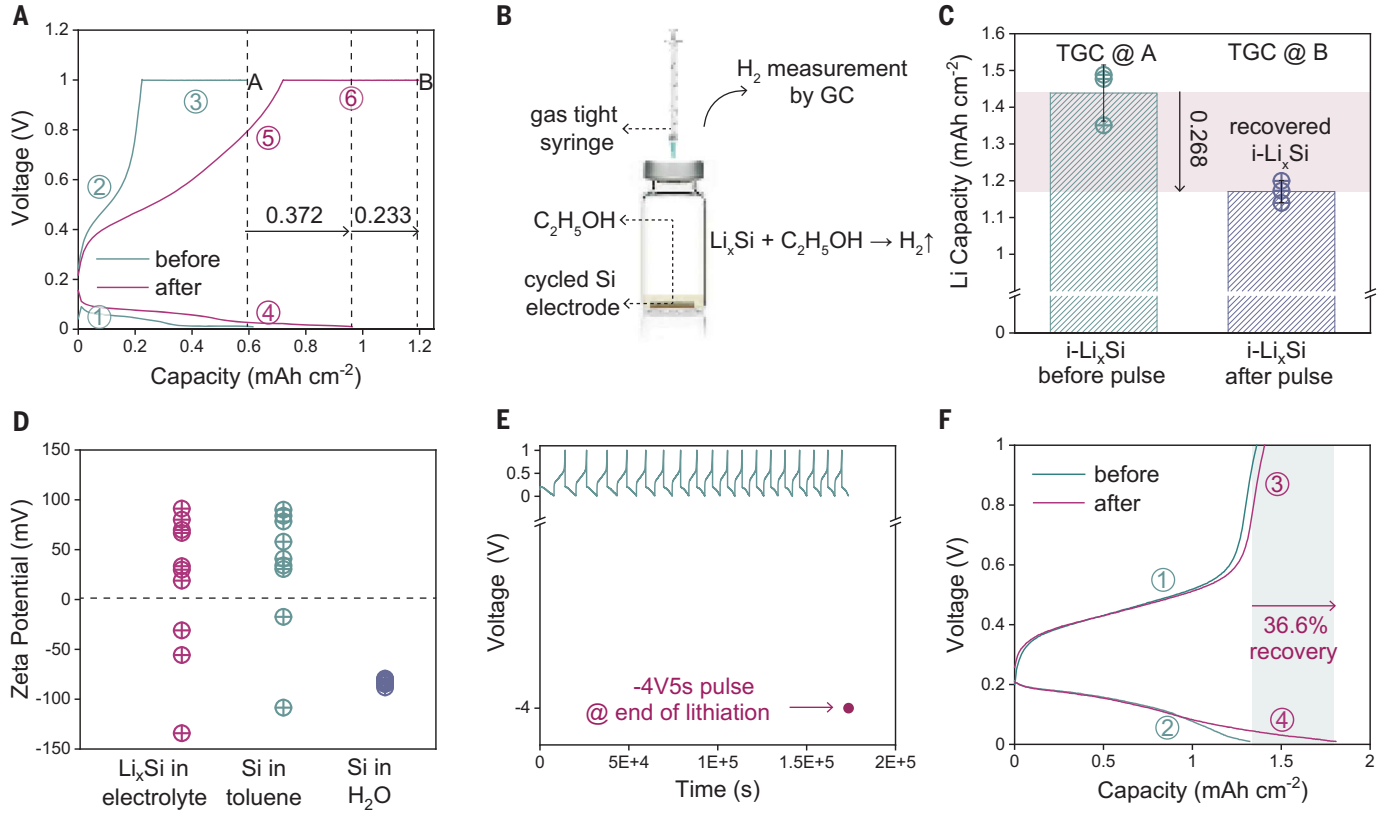

Fig. 3. Verification of the i-Li$_x$Si recovery via the DEP mzechanism. (**A**) Voltage-capacity profiles before and after the 4-V, 5-s pulse at the 20th cycle under the CCCV protocol. The numbers indicate the sequence of the protocol. The letters label different states of the Si anode. The vertical dashed lines are drawn to guide the eye. (**B**) The schematics of the TGC setup. (**C**) The statistics of the titration result at post-CV steps in the cycle before the pulse (state A) and after the pulse (state B). Each colored circle represents one cell, the box shows the average value, and the error bars indicate the standard deviation. Li capacity before the pulse was measured as 1.439 ± 0.076 mA·hour cm^{-2}, and Li capacity after the pulse was measured 1.171 ± 0.030 mA·hour cm^{-2}. (**D**) The PLAS-measured zeta potentials of Li$_x$Si particles in electrolyte, Si nanoparticles in toluene, and Si nanoparticles in H_2O (pH = 7), respectively. Each colored circle represents one measurement. (**E**) Voltage-time profiles of negative pulse application to Li-Si cells. (**F**) Voltage-capacity profiles of Li-Si cells before and after the negative 4-V, 5-s pulse at the 20th cycle. The order is indicated by numbers.

DEP is expected, and we observed that the Li$_x$Si particle was attracted to the tip (Fig. 4B). This attraction was not because the Li$_x$Si particle was negatively charged, because the repulsion was also observed before the attraction on the same particle (movies S1 and S2). This operando observation demonstrates the i-Li$_x$Si movement in the nonuniform electric field. To better reproduce the real-cell condition, an optical cell was fabricated for operando observation of i-Li$_x$Si movement within the electrolyte under the voltage pulse (Fig. 4C and fig. S13). A similar setup with a tungsten tip and a Cu foil as two electrodes was used, and a 4-V constant voltage was applied to the tungsten tip. The i-Li$_x$Si suspension was made by scratching off the cycled Si anode surface and adding those particles to the electrolyte. Diffusive fluxes within the electrolyte resulted in the random flow behavior of tiny particles, but large particles stayed still before voltage application (movie S3). Particles were labeled as a, b, and c to keep track of their movement. After applying the voltage pulse, the labeled particles showed evident movement (Fig. 4D). The motion of the tiny particles was also accelerated under the pulse. Some larger particles stayed motionless, possibly because they remained as sediments on the substrate owing to their higher mass. Observations from the optical cell reaffirmed the migration of i-Li$_x$Si particles during the voltage pulse within the electrolyte.

Numerical simulation

Additionally, we performed numerical modeling to understand the isolated Li$_x$Si movement more specifically using the commercial finite element software COMSOL Multiphysics. The electro-DEP-fluid model used for tracing i-Li$_x$Si movement under the voltage pulse is presented in Fig. 4E (pulse time = 0 s). A constant voltage of 4 V was applied to an active Si particle (represented by the white semisphere), and the electric field density is illustrated through the color contour. A line of i-Li$_x$Si particles is represented by the yellow spheres, which simulates isolated Li$_x$Si at different initial distances away from the active Si. In practical battery electrodes, isolated Li$_x$Si with varied lithiation degrees exists, and thus we simulated two extreme conditions of fully lithiated i-Li$_x$Si (x = 3.75) and nonlithiated i-Li$_x$Si (x = 0). Figure 4F and movie S4 demonstrate the movement of fully lithiated i-Li$_x$Si particles, where particle trajectories are shown by the yellow lines. Once the pulse was applied, the i-Li$_x$Si particles experienced positive DEP and moved toward the electric field with higher density. Figure 4G and movie S5 depict the negative DEP condition in which i-Li$_x$Si particles are nonlithiated. The i-Li$_x$Si particles moved toward lower electric field density (i.e., away from the active particle). For a quantitative understanding of the traversed distance, we take particle A and particle B as examples, which represent i-Li$_x$Si at a small initial distance (5 μm) and a large initial distance (23 μm), respectively. Their displacement within the 4-V, 5-s pulse is specified in Fig. 4H. Positive

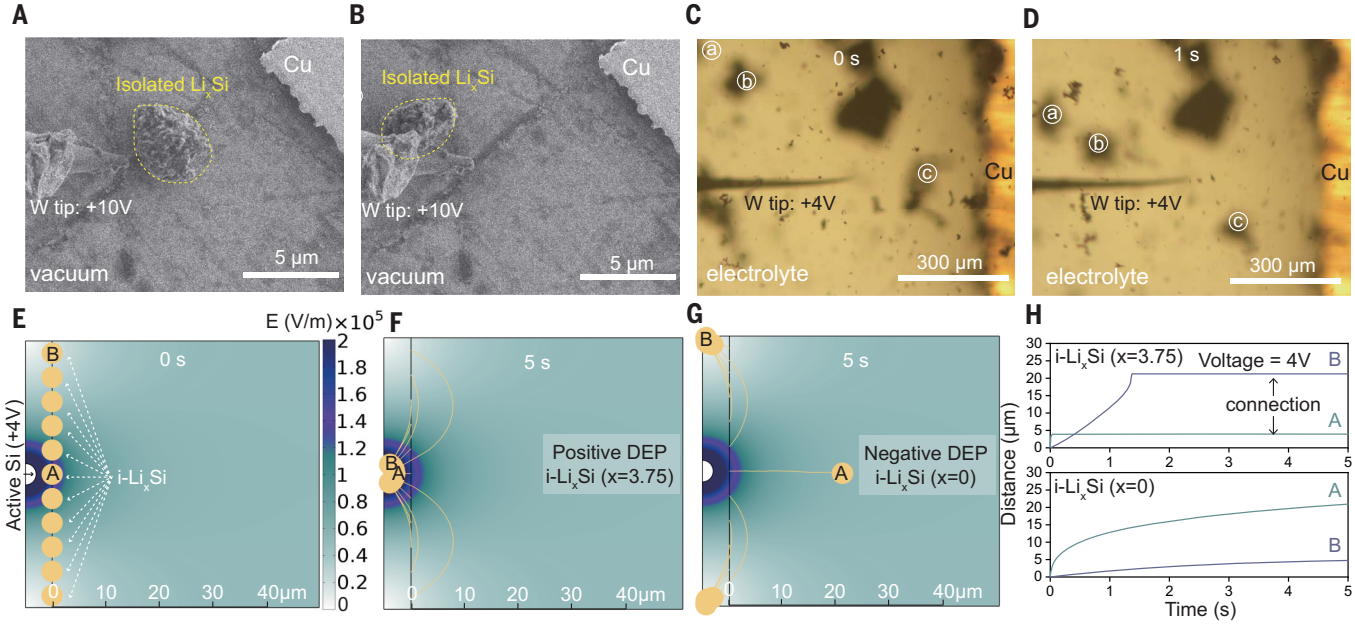

Fig. 4. Migration of isolated Li_xSi under the voltage pulse. (**A** and **B**) In situ SEM observations of isolated Li_xSi movement under the nonuniform electric field. (**C** and **D**) Operando optical observations of isolated Li_xSi suspended in the electrolyte under the voltage pulse at 0 s (C) and 1 s (D). The letters label the particle positions before and after the voltage pulse. (**E**) An electro-DEP-fluid model for tracing isolated particle movements at 0 s; the color contour illustrates the electric field density. (**F** and **G**) The trajectories of isolated Li_xSi particles under the voltage pulse: positive DEP [i-Li_xSi (x = 3.75), time equal to 5 s] (F) and negative DEP [i-Li_xSi (x = 0), time equal to 5 s] (G). (**H**) Traversed distance of two representative particles (labeled A and B) under the voltage pulse for both positive DEP (top) and negative DEP (bottom).

DEP allowed immediate reconnection of particle A in 0.1 s and particle B within 1.5 s. In negative DEP, particle A traveled more than 20 μm during a 4-V, 5-s pulse, and B traveled nearly 5 μm. These scales of the traversed distances promisingly result in reconnection within tightly packed electrodes.

Pulse application to full battery

The practical application of the voltage pulse has been demonstrated in the Si–lithium iron phosphate (Si-LFP) full-cell configuration. Similar to the half-cell protocol, a 4-V pulse was applied for 5 s on the Si side [cell voltage (LFP versus Si) = −4 V] at the end of delithiation in the 20th cycle (Fig. 5A). A recovery of 31.9%, from 1.066 to 1.406 mA·hour cm^{-2}, was obtained (Fig. 5B and fig. S14, A and B), indicating that pulse-induced recovery applies to the full batteries. A three-electrode system was further designed to understand the voltage distribution during the pulse (Fig. 5C). A small piece of Li metal connected by Cu wire was placed between Si and LFP, acting as the reference electrode. The voltage pulse was applied between the Si anode and the LFP cathode while the open-circuit voltage (OCV) between the anode and the reference electrode was tracked. Figure 5D illustrates the measured voltage distribution. When driving the LFP versus Si potential to −4 V, the potential of Si versus Li reference increases with time from 2.5 to 4.7 V. The potential of LFP versus Li thus can be calculated, increasing from −1.5 to 0.7 V. The negative LFP versus Li potential only lasts for 2 s, and no Li metal aggregates on LFP are observed after the pulse (fig. S15). The impedance measurements also revealed negligible changes in both R_{ohm} and R_{SEI} after the pulse, suggesting that Li plating is unlikely to occur within the LFP electrodes (fig. S14, C and D). The stabilities of the LFP electrodes, Al current collectors, and Cu current collectors were evaluated, revealing no noticeable difference before and after the pulse (figs. S16 to S19). Supplementary to the pulse applied after the initial 20 cycles, we applied sequential voltage pulses at the 100th, 120th, and 140th cycles, yielding capacity recoveries of 15.2, 20.0, and 10.1%, respectively. The recurring recovery resulted in improved capacity, consistently surpassing that of the cell without pulse application. The recovery at later cycles in the full cell was less pronounced than in the half cell. This phenomenon can be attributed to the continuous SEI formation, which gradually depletes the limited active Li in the full cells, resulting in insufficient active Li to activate reconnected isolated $Li_\alpha Si$. Pulse-induced capacity recovery has also been studied and demonstrated in the pouch-cell system, expanding the potential of our pulse approach for practical applications (fig. S20). Overall, this work presents a pioneering approach to recover the lost active materials in Si electrodes, opening new opportunities to extend the cycle life in high-capacity electrode materials.

REFERENCES AND NOTES

1. M. Armand, J.-M. Tarascon, *Nature* **451**, 652–657 (2008).
2. M. Li, J. Lu, Z. Chen, K. Amine, *Adv. Mater.* **30**, e1800561 (2018).
3. S. Chu, Y. Cui, N. Liu, *Nat. Mater.* **16**, 16–22 (2016).
4. M. T. McDowell, S. Xia, T. Zhu, *Extreme Mech. Lett.* **9**, 480–494 (2016).
5. L. Y. Beaulieu, K. W. Eberman, R. L. Turner, L. J. Krause, J. R. Dahn, *Electrochem. Solid-State Lett.* **4**, A137 (2001).
6. Y. Liu, G. Zhou, K. Liu, Y. Cui, *Acc. Chem. Res.* **50**, 2895–2905 (2017).
7. Y. Cui, *Nat. Energy* **6**, 995–996 (2021).
8. P. G. Bruce, S. A. Freunberger, L. J. Hardwick, J.-M. Tarascon, *Nat. Mater.* **11**, 19–29 (2011).
9. P. Albertus, S. Babinec, S. Litzelman, A. Newman, *Nat. Energy* **3**, 16–21 (2018).
10. N. Kim, Y. Kim, J. Sung, J. Cho, *Nat. Energy* **8**, 921–933 (2023).
11. J.-i. Yamaki *et al.*, *J. Power Sources* **74**, 219–227 (1998).
12. A. Pei, G. Zheng, F. Shi, Y. Li, Y. Cui, *Nano Lett.* **17**, 1132–1139 (2017).
13. K.-H. Chen *et al.*, *J. Mater. Chem. A Mater. Energy Sustain.* **5**, 11671–11681 (2017).
14. S. Xu, K.-H. Chen, N. P. Dasgupta, J. B. Siegel, A. G. Stefanopoulou, *J. Electrochem. Soc.* **166**, A3456–A3463 (2019).
15. Y. Li *et al.*, *Joule* **2**, 2167–2177 (2018).
16. M. T. McDowell, S. W. Lee, W. D. Nix, Y. Cui, *Adv. Mater.* **25**, 4966–4985 (2013).
17. S. Müller *et al.*, *Nat. Commun.* **9**, 2340 (2018).
18. D. Lin, Y. Liu, Y. Cui, *Nat. Nanotechnol.* **12**, 194–206 (2017).
19. J. Liu *et al.*, *Nat. Energy* **4**, 180–186 (2019).
20. J. W. Choi, D. Aurbach, *Nat. Rev. Mater.* **1**, 16013 (2016).
21. N. Liu *et al.*, *Nat. Nanotechnol.* **9**, 187–192 (2014).
22. Y. Li *et al.*, *Nat. Energy* **1**, 15029 (2016).
23. D. Lin *et al.*, *Nat. Nanotechnol.* **11**, 626–632 (2016).
24. H. Wu *et al.*, *Nat. Nanotechnol.* **7**, 310–315 (2012).
25. Y. Gao *et al.*, *Nat. Mater.* **18**, 384–389 (2019).
26. Z. Huang *et al.*, *Nat. Energy* **8**, 577–585 (2023).
27. J. Chen *et al.*, *Nat. Energy* **5**, 386–397 (2020).
28. D. H. S. Tan *et al.*, *Science* **373**, 1494–1499 (2021).
29. Z. Yu *et al.*, *Nat. Energy* **5**, 526–533 (2020).
30. Z. Zeng *et al.*, *Nat. Energy* **3**, 674–681 (2018).
31. C. Jin *et al.*, *Nat. Energy* **6**, 378–387 (2021).
32. F. Liu *et al.*, *Nature* **600**, 659–663 (2021).

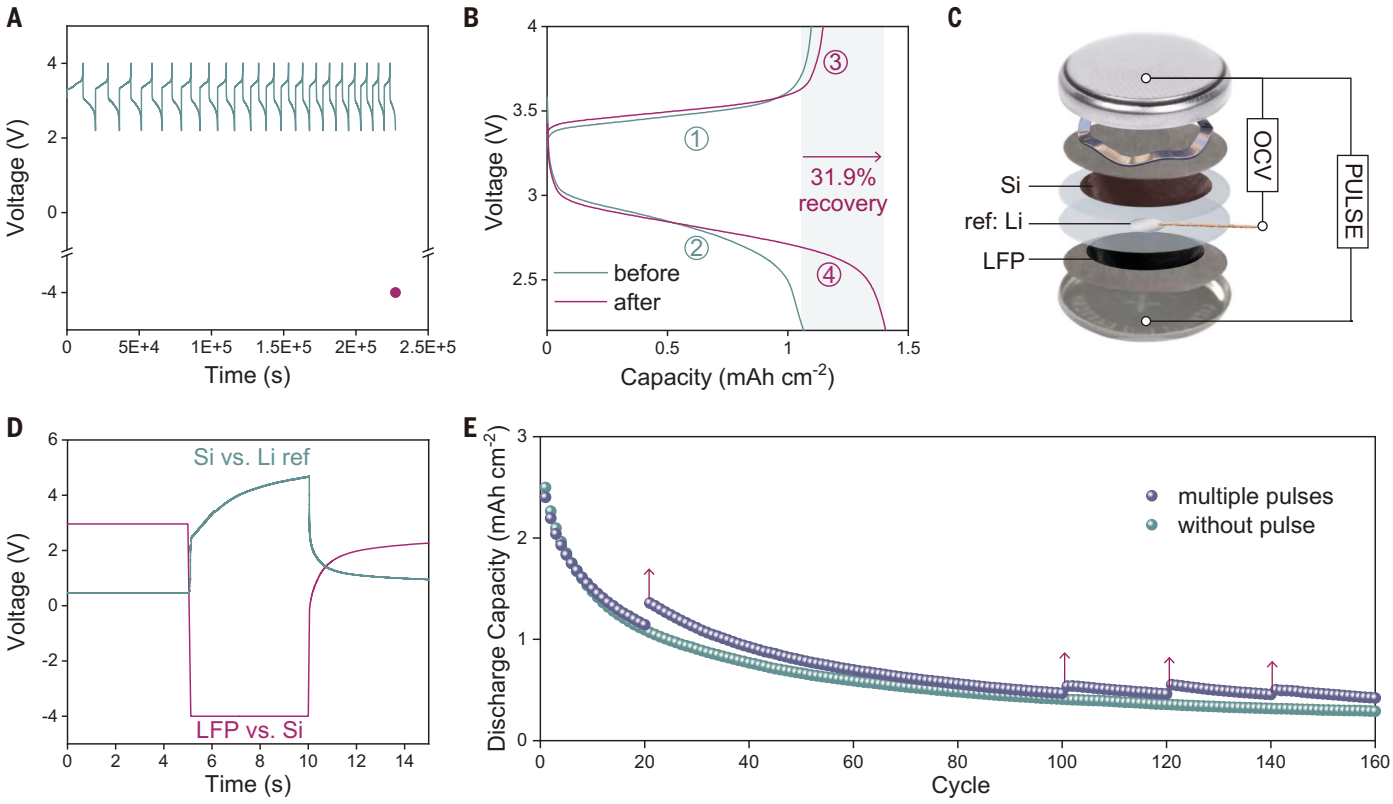

Fig. 5. Capacity recovery in Si-based full-cell batteries. (**A**) Voltage-time profiles of Si-LFP cells, illustrating the pulse-application profile. (**B**) Voltage-capacity profiles of Si-LFP cells before and after the voltage pulse at the 20th cycle. The order is indicated by numbers. (**C**) Three-electrode configuration of a Si-LFP cell with a piece of Li foil in between as the reference electrode. The pulse was applied between the Si and LFP electrodes while measuring the OCV between the Si and Li reference. (**D**) Voltage-time profiles of LFP versus Si and Si versus Li reference during the voltage pulse. (**E**) Repeatable capacity recovery of Si-LFP full cells with multiple pulses at the 20th, 100th, 120th, and 140th cycles.

33. W. Zhang *et al.*, *Nature* **626**, 306–312 (2024).
34. B. Çetin, D. Li, *Electrophoresis* **32**, 2410–2427 (2011).
35. H. Morgan, M. P. Hughes, N. G. Green, *Biophys. J.* **77**, 516–525 (1999).
36. H. A. Pohl, J. S. Crane, *Biophys. J.* **11**, 711–727 (1971).
37. N. G. Green, H. Morgan, *J. Phys. D Appl. Phys.* **30**, L41–L44 (1997).
38. E. M. Freer, O. Grachev, X. Duan, S. Martin, D. P. Stumbo, *Nat. Nanotechnol.* **5**, 525–530 (2010).
39. M. Dürr, J. Kentsch, T. Müller, T. Schnelle, M. Stelzle, *Electrophoresis* **24**, 722–731 (2003).
40. W. Bao *et al.*, *Cell Rep. Phys. Sci.* **2**, 100597 (2021).
41. B. Sreenarayanan *et al.*, *J. Power Sources* **531**, 231327 (2022).
42. C. O. Metin, J. R. Baran Jr., Q. P. Nguyen, *J. Nanopart. Res.* **14**, 1246 (2012).

ACKNOWLEDGMENTS

We acknowledge the use and support of the Stanford Nano Shared Facilities (SNSF) and the Stanford Nanofabrication Facility (SNF), which are supported by the National Science Foundation under awards ECCS-2026822 and ECCS-1542152. We thank J. N. Weker for insightful discussions. Y.C. (corresponding author) acknowledges the Hydro-Québec company for providing the commercialized 25-μm-thick pure Li metal foil. **Funding:** This work was financially supported by the Assistant Secretary for Energy Efficiency and Renewable Energy, Office of Vehicle Technologies of the US Department of Energy, under the Battery Materials Research program; and the Office of Basic Energy Sciences, US Department of Energy, Division of Materials Science and Engineering, DE-AC02-76SF00515. **Author contributions:** Y.C. (corresponding author), Y. Yang, and S.B. conceived the idea for the project and designed the experiments. Y. Yang. and S.B. conducted the electrochemical characterizations. R.X. conducted numerical simulations. X. Xu conducted the in situ SEM experiments. Y. Yang and S.B. conducted the optical cell experiments. X. Xin conducted the TGC characterizations. Y. Yang performed SEM and XPS characterizations. H.G. conducted the zeta potential measurements. H.A. built and tested the pouch cells. J.L., C.S., W.Z., and Y.C. conducted the cryo-TEM and cryo–electron energy-loss spectroscopy characterizations. P.Z., Y. Ye, Y.W., X.Z., W.Z., P.S., and Z.C. designed and conducted experiments for mechanism verification. X.G., Y.P., Z.H., R.A.V., and D.T.B. provided insight into mechanism exploration. Y. Yang, S.B., and Y.C. (corresponding author) wrote and revised the manuscript with input from all authors. All authors took part in the scientific discussions at all stages. **Competing interests:** The authors declare that they have no competing interests. **Data and materials availability:** All data needed to evaluate the conclusions in this paper are present in the paper or the supplementary materials.

SUPPLEMENTARY MATERIALS

science.org/doi/10.1126/science.adn1749
Materials and Methods
Supplementary Text
Figs. S1 to S20
Table S1
References (*43*–*47*)
Movies S1 to S5

Submitted 1 December 2023; resubmitted 3 July 2024
Accepted 12 August 2024
10.1126/science.adn1749

Capacity recovery by transient voltage pulse in silicon-anode batteries

Yufei Yang, Srija Biswas, Rong Xu, Xin Xiao, Xin Xu, Pu Zhang, Huaxin Gong, Xueli Zheng, Yucan Peng, Junyan Li, Huayue Ai, Yecun Wu, Yusheng Ye, Xin Gao, Chad Serrao, Wenbo Zhang, Philaphon Sayavong, Zhuojun Huang, Zhouyi Chen, Yi Cui, Rafael A. Vilá, David T. Boyle, and Yi Cui

Science **386** (6719), . DOI: 10.1126/science.adn1749

Editor's summary

Capacity loss in silicon electrodes occurs due to volume change upon lithiation and associated problems with solid electrolyte interphase formation, which can cause isolated, inactive lithium silicide (LiSi) particles to form. Yang *et al*. applied high voltages for short periods of time (a few seconds) as a way to recover lost capacity (see the Perspective by Jin and Tao). The voltage pulses cause dielectrophoresis to move the disconnected LiSi particles such that the lithium is reactivated. Pulsing can be applied repeatedly to substantially recover lost capacity over the lifetime of a cell. —Marc S. Lavine